UC Irvine
UC Irvine Previously Published Works

Title
Enhanced photo-sono therapy with dual-frequency ultrasound

Permalink
https://escholarship.org/uc/item/8qw9j2hc

Journal
APL Bioengineering, 9(4)

ISSN
2473-2877

Authors
Song, Yuchen
Wei, Shuang
Zou, Haibin
et al.

Publication Date
2025-12-01

DOI
10.1063/5.0288979

Copyright Information
This work is made available under the terms of a Creative Commons Attribution License, available at https://creativecommons.org/licenses/by/4.0/

Peer reviewed

eScholarship.org Powered by the California Digital Library
University of California

APL Bioengineering

RESEARCH ARTICLE | OCTOBER 30 2025

Enhanced photo-sono therapy with dual-frequency ultrasound

Yuchen Song ; Shuang Wei ; Haibin Zou ; Jingyi Wang ; Fengyi Zhang ; Qifa Zhou ; Yun Jing ; Zhongping Chen

Check for updates

APL Bioeng. 9, 046109 (2025)
https://doi.org/10.1063/5.0288979

View Online
Export Citation

Connected Content

A companion article has been published: Enhancing cavitation-based anti-vascular and thrombolysis therapy

Articles You May Be Interested In

Enhancing cavitation-based anti-vascular and thrombolysis therapy

Scilight (October 2025)

One pot sono-chemical synthesis of 2D layered MoS_2 nanosheets

AIP Conf. Proc. (May 2016)

Enhanced photo-, sono- and sonophotocatalysis of methylene blue via SnO_2 nanoparticle supported on nanographene platelets (NGP)

AIP Conf. Proc. (July 2017)

06 November 2026 22:47:50



AIP Publishing

APL Bioengineering ARTICLE pubs.aip.org/aip/apb

Enhanced photo-sono therapy with dual-frequency ultrasound

Cite as: APL Bioeng. **9**, 046109 (2025); doi: 10.1063/5.0288979
Submitted: 4 July 2025 · Accepted: 28 September 2025 ·
Published Online: 30 October 2025

View Online Export Citation CrossMark

Yuchen Song,[1,2] Shuang Wei,[1,2] Haibin Zou,[1] Jingyi Wang,[1,3] Fengyi Zhang,[1,2] Qifa Zhou,[4] Yun Jing,[5,a)] and Zhongping Chen[1,2,3,a)]

AFFILIATIONS

[1]Beckman Laser Institute, University of California Irvine, Irvine, California 92612, USA
[2]Department of Biomedical Engineering, University of California Irvine, Irvine, California 92612, USA
[3]Department of Electrical Engineering and Computer Science, University of California Irvine, Irvine, California 92612, USA
[4]Department of Biomedical Engineering, University of Southern California, Los Angeles, California 90089, USA
[5]Graduate Program in Acoustics, The Pennsylvania State University, University Park, Pennsylvania 16802, USA

[a)]**Authors to whom correspondence should be addressed:** yqj5201@psu.edu and z2chen@uci.edu

ABSTRACT

Photo-sono therapy (PST) is a cavitation-based anti-vascular and thrombolysis treatment strategy. Compared to conventional high intensity focused ultrasound treatment, PST can selectively treat blood vessels and clots because of optical absorption. Current methods typically combine a single-frequency ultrasound burst with pulse laser irradiation. However, the high acoustic energy required and limited treatment efficacy present a barrier to the clinical application of this technique. In this paper, we introduce a dual-frequency ultrasound approach to enhance PST efficacy with reduced acoustic energy. Through both theoretical bubble dynamics modeling and experimental study, the effect of dual-frequency ultrasound in PST is evaluated. The feasibility of the proposed method was validated using *ex vivo* blood vessel and blood clot phantoms, as well as an *in vivo* rabbit model. Results show that dual-frequency PST enhances cavitation activity, thrombolysis, and anti-vascular efficiency, highlighting its potential for clinical translation.

© 2025 Author(s). All article content, except where otherwise noted, is licensed under a Creative Commons Attribution-NonCommercial 4.0 International (CC BY-NC) license (https://creativecommons.org/licenses/by-nc/4.0/). https://doi.org/10.1063/5.0288979

06 November 2026 22:47:50

INTRODUCTION

High intensity focused ultrasound (HIFU) is rapidly gaining clinical acceptance as a technique capable of providing non-invasive therapy for a wide range of applications, including thrombolysis and tissue ablation.[1–3] Cavitation serves as a primary mechanism underlying the therapeutic effects of HIFU, and acoustic cavitation is strongly dependent on ultrasound (US) frequency.[4–6] Low-frequency (<1 MHz) transducers are commonly selected for treatment; however, they can result in poor spatial resolution and increase the risk of damage to blood vessels and surrounding tissues. In addition, the high acoustic energy required for HIFU treatment (typically on the order of tens to hundreds MPa peak pressure) raises concerns about unintended thermal injury to adjacent tissues, posing challenges for broader clinical applications.[3,7]

Photo-sono therapy (PST) is a novel cavitation-based anti-vascular technique that simultaneously applies nanosecond laser pulses and ultrasound bursts to enhance cavitation activity for blood vessel removal.[8–10] Cavitation probability is strongly dependent on the peak negative pressure. In PST, a nanosecond laser pulse generates a photoacoustic (PA) wave that can be time-delayed to overlap with the negative phase of the ultrasound burst, thereby lowering the cavitation threshold. Lateral synchronization is achieved by confocal alignment of the laser and US focus, while axial selectivity is controlled by choosing the specific US cycle with which the laser pulse is synchronized. Hence, by precisely synchronizing the spatiotemporal overlap of laser-induced photoacoustic waves and ultrasound bursts, selective cavitation can be induced within targeted tissues.[11] Additionally, PST minimizes damage to the epidermis and surrounding tissues by requiring significantly lower laser and ultrasound energy compared to conventional therapies that apply laser or ultrasound alone.[12] Laser fluence can be reduced to tens of mJ/cm^2 range, compared with several J/cm^2 per pulse in traditional pulsed dye laser treatment, while the required ultrasound intensity is below hundreds of kPa, both lower than those used in conventional pulsed laser or HIFU therapies. However, current PST treatment with single-frequency ultrasound typically takes several minutes to ablate vessels at a single site.

© Author(s) 2025

Dual-frequency sonication has recently been reported as a powerful strategy for enhancing ultrasound-based therapeutics.[13–15] By combining two different ultrasound frequencies, studies have demonstrated that dual-frequency ultrasound can enhance cavitation activity and improve therapeutic outcomes in applications such as thrombolysis and ablation.[16–19] Moreover, dual-frequency approaches can achieve comparable or better treatment effects at lower acoustic power levels, reducing the risk of unwanted thermal damage to surrounding tissues. Hence, we propose to combine dual-frequency ultrasound with pulse laser to further enhance the treatment efficiency of PST while minimizing ultrasound power requirements.

In this study, we developed a PST system based on dual-frequency sonication to enhance treatment efficiency and reduce the required acoustic energy. Meanwhile, optical coherence tomography (OCT) was integrated to evaluate the performance of PST. We first estimated the cavitation threshold of dual-frequency PST through theoretical simulation by solving the bubble dynamics equations and compared it with single-frequency PST and ultrasound-only conditions. To demonstrate the feasibility of the proposed system, we evaluated cavitation activity using passive cavitation detection (PCD) in *ex vivo* blood phantoms. Finally, we validated the therapeutic improvements through experiments in *ex vivo* blood clot phantoms and *in vivo* rabbit model. Our results show that PST enhances thrombolytic efficacy with greater precision than HIFU and that dual-frequency PST further amplifies inertial cavitation and improves overall treatment efficiency.

RESULTS

The schematic of the proposed dual-frequency PST system integrated with OCT is shown in Fig. 1(a). The corresponding timing diagram for single- and dual-frequency PST excitation is illustrated in Fig. 1(b). Function generator produced 20 cycles sine wave bursts every 400 μs, corresponding to a 10% duty cycle. The carrier frequency was set to 500 kHz for the single-frequency mode, or to a combination of 500 and 525 kHz for the dual-frequency mode. A delay generator is then used to introduce a time delay to the laser pulse. The total delay is equal to the ultrasound travel time plus the interval from the start of the dual-frequency burst to its strongest negative pressure peak. To ensure equal acoustic energy per cycle between the single- and dual-frequency excitations, the peak negative pressure p_{peak} of the dual-frequency signal was set to be $\sqrt{2}$ times higher than that of the single-frequency signal,[16] as shown in Fig. 1(c). All ultrasound pressures reported in the following simulations and experiments refer to peak negative pressure p_{peak}. For single-frequency excitation, the applied pressure is p_{peak}, while for dual-frequency excitation, the corresponding peak negative pressure is $\sqrt{2}\,p_{peak}$.

To understand the underlying mechanism by which dual-frequency PST enhances cavitation activity, we simulated single bubble

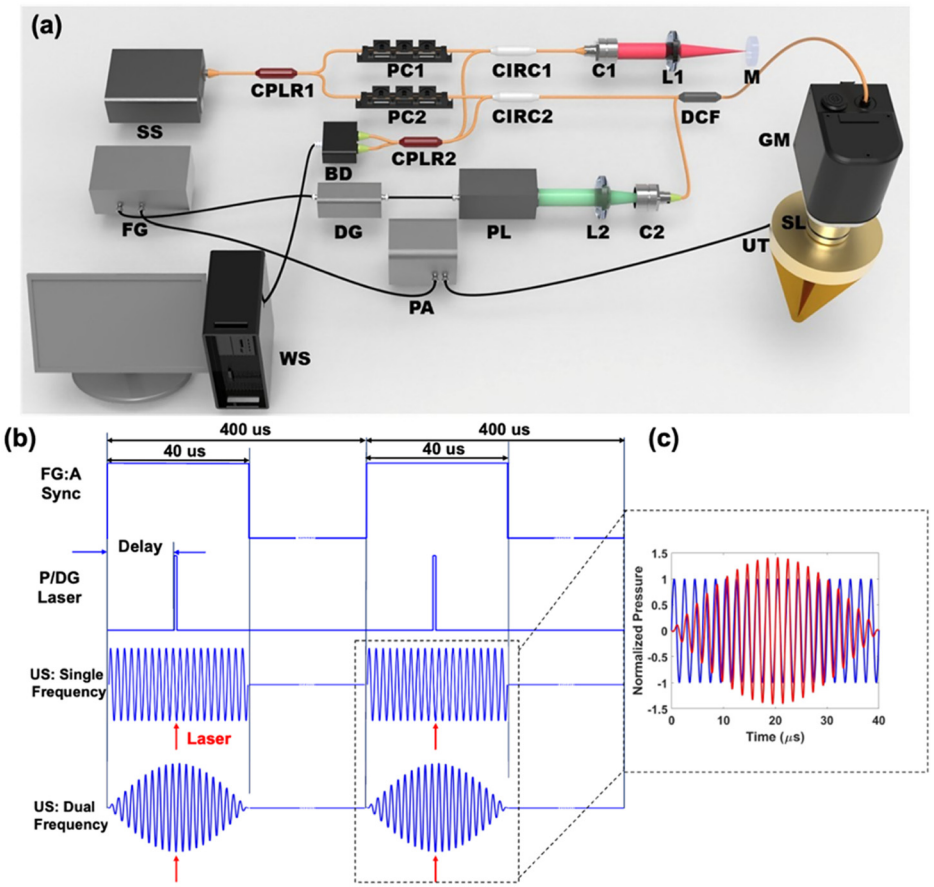


FIG. 1. Overview of the OCT-guided dual-frequency PST system. (a) Schematic of the dual-frequency PST system integrated with OCT for imaging guidance and monitoring. FG: function generator; WS: workstation; BD: balance detector; DG: delay generator; PA: power amplifier; PL: pulsed laser; SS: sweep source laser; GM: galvanometric mirror; SL: scanning lens; UT: ultrasound transducer; PC: polarization controller; CPLR: coupler; CIRC: circulator; DCF: double-clad fiber; L: lens; C: coupler. (b) Timing diagram for single- and dual-frequency ultrasound burst excitations synchronized with pulsed laser irradiation. P/DG: pulse delay generator. (c) Acoustic waveforms of single- and dual-frequency bursts.

06 November 2026 22:47:50

© Author(s) 2025

dynamics under various laser and acoustic conditions based on the Keller–Miksis model.[20,21] The model computed the bubble radius R as a function of time, and the normalized radius R/R_0 was used to evaluate bubble dynamics. Inertial cavitation is defined to occur when the maximum normalized radium $R_{max}/R_0 \geqq 2$.[20] As shown in Fig. 2(a), 500 kHz ultrasound burst alone at 0.5 kPa does not induce inertial cavitation. When both ultrasound and pulsed laser irradiation (10 mJ/cm^2) are applied [Fig. 2(b)], the bubble expands beyond the inertial cavitation threshold. Figure 2(c) compares the cavitation thresholds across ultrasound-only, single-frequency PST, and dual-frequency PST conditions. Notably, dual-frequency PST requires approximately half the peak negative pressure p_{peak} of single-frequency PST to achieve inertial cavitation, demonstrating a significantly lower threshold. Figure 2(d) further illustrates the relationship between cavitation threshold and laser influence under dual-frequency conditions, showing that increasing laser energy leads to a lower acoustic

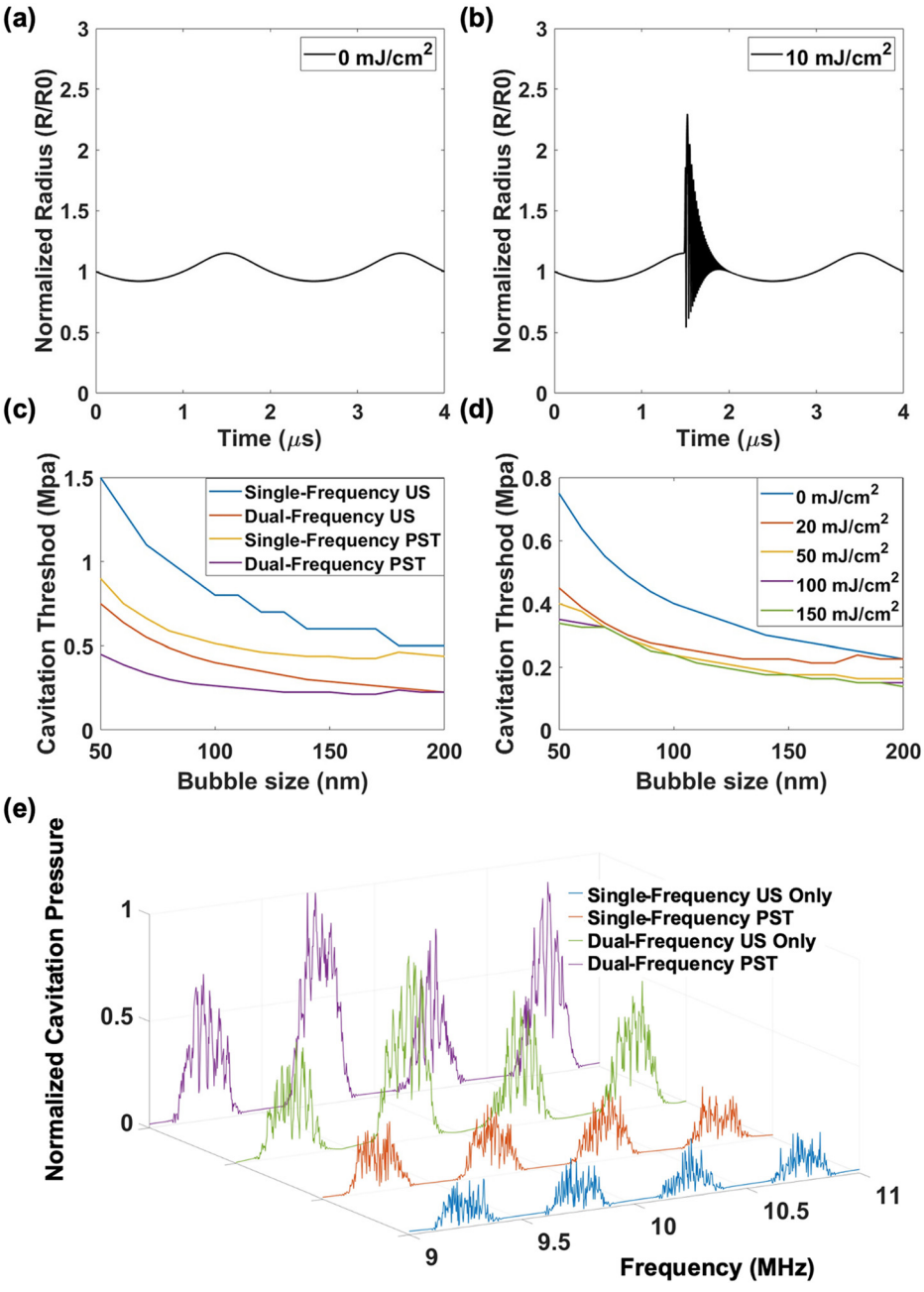


FIG. 2. Simulation of cavitation activities based on Keller–Miksis model. (a) Bubble radius changes with US only at 0.5 MPa. (b) Bubble radius changes under PST (US at 0.5 MPa + pulse laser at 10 $\frac{mJ}{cm^2}$). (c) Comparison of cavitation threshold with single-frequency PST, dual-frequency PST, and US only. (d) Comparison of cavitation threshold with different laser fluences. (e) Experimental results of cavitation activities with PCD detection in blood vessel phantom. Harmonic and subharmonic frequencies for 500 and 525 kHz are filtered.

06 November 2026 22:47:50

© Author(s) 2025

threshold for cavitation initiation. Experimental validation using passive cavitation detection (PCD) in *ex vivo* blood vessel phantoms (with a comb notch filter applied) is shown in Fig. 2(e). These results confirm that dual-frequency PST produces the highest cavitation activity under identical ultrasound and laser energy inputs, in agreement with the simulation outcomes.

Following simulation validation, we assessed thrombolytic efficacy through *ex vivo* experiments using blood clot phantoms. A self-built sweep source optical coherence tomography (SS-OCT) system [Fig. 1(a)] was used to acquire 3D structural images of the clots before and after ultrasound treatment, allowing quantitative estimation of clot dispersion. Representative top and side views of the blood clot after ultrasound-only treatment are shown in Figs. 3(a) and 3(b), respectively, with a 3D reconstruction presented in Fig. 3(c). The ultrasound exposure time was fixed at 30 s for both single- and dual-frequency conditions across varying ultrasound power levels. Each experimental group included six samples. As shown in Fig. 3(d), single- frequency ultrasound resulted in minimal thrombolytic effect at low p_{peak} (333 kPa), while dual-frequency ultrasound achieved noticeable clot dispersion. Across all tested p_{peak} levels, dual-frequency ultrasound consistently produced significantly greater thrombolytic effects compared to single-frequency treatment.

We further investigate the thrombolytic performance by combining pulsed laser irradiation with both single- and dual-frequency focused ultrasound. The pulse laser was applied at a fluence of 2 mJ/cm^2, with 2.5 kHz repetition rate, a setting that only produced minimal surface damage to the clot [Fig. 4(a)]. Ultrasound peak pressures p_{peak} were set to 400 kPa; under these conditions, ultrasound alone did not induce significant clot dispersion [Fig. 4(b)]. However, when combined with pulsed laser irradiation, a marked improvement in thrombolysis was observed [Fig. 4(c)]. To compare treatment efficacy, five groups were tested with 30 s of exposure per treatment and a sample size of six per group. Statistical results in Fig. 4(e) demonstrate that effective thrombolysis only occurred when both ultrasound and laser were applied, with dual-frequency PST outperforming single-frequency PST. To assess the precision of treatment, Fig. 4(d) compares dual-frequency PST at p_{peak} of 400 kPa with dual-frequency ultrasound-only at p_{peak} of 600 kPa. While both achieved similar thrombolytic depth, dual-frequency PST resulted in a narrower treatment zone, suggesting improved spatial precision. The treatment diameter is consistent with the beam profile of the pulsed laser. Figure 4(f) presents the statistical analysis of thrombolysis depth and diameter, confirming that PST enhances treatment localization while reducing the required ultrasound power.

To further validate the therapeutic efficacy of dual-frequency PST, *in vivo* experiments were conducted on rabbit ear vasculature. Each treatment site was treated with pulsed laser fluence of 2 mJ/cm^2 and p_{peak} of 400 kPa. The total treatment duration per site was 10 s. Treatment outcomes were compared across different conditions, with a total of 30 treatment sites imaged from four rabbits. Optical coherence tomography angiography (OCTA) was performed before and after treatment to assess changes in vessel structures. Representative OCTA images before and after dual-frequency ultrasound-only treatment are shown in Figs. 5(a) and 5(b). No apparent changes in vascular structure were observed under ultrasound-only conditions, regardless of vessel size or depth. In contrast, the addition of laser irradiation at the same ultrasound pressure led to clear destruction of targeted blood vessels, as seen in Figs. 5(c) and 5(d). OCTA results show that the diameters of destroyed blood vessels range from a few micrometers to several hundred micrometers. The temperature change during PST treatment was measured as shown in Figs. 5(e) and 5(f). The results indicate that the tissue temperature in rabbit ears increased by approximately 3–6 °C. Treatment outcomes were classified as successful if vessel density decreased or blood vessel destruction was observed. A summary of outcomes across all treatment groups is provided in Table I. Only the single- and dual-frequency PST conditions produced successful outcomes under the low-power laser and ultrasound settings. Neither ultrasound nor laser alone was sufficient to destroy blood vessels. Furthermore, dual-frequency PST showed an improved treatment success rate compared to single-frequency PST.

DISCUSSION

In summary, we demonstrated that PST enhances cavitation activity and improves treatment efficiency with greater spatial precision compared to HIFU alone. More importantly, dual-frequency PST further increases therapeutic efficacy compared to single-frequency PST. Both the *ex vivo* thrombolysis experiments and the *in vivo* antivascular treatment in rabbit ears confirm the superior performance of dual-frequency PST, in agreement with theoretical simulations. This

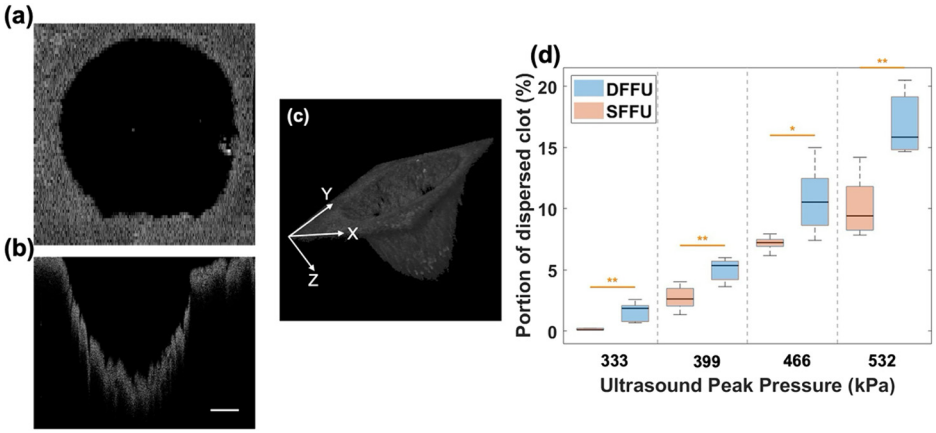


FIG. 3. *Ex vivo* evaluation of thrombolysis performance using single- and dual-frequency focused ultrasound. (a) Top-view and (b) side-view OCT images of a blood clot phantom after ultrasound-only treatment. (c) 3D reconstruction of the clot. (d) T-test comparison of thrombolysis efficiency under different ultrasound peak pressures using single-frequency focused ultrasound (SFFU, orange) and dual-frequency focused ultrasound (DFFU, blue). For DFFU, the actual peak pressure is $\sqrt{2}$ times the ultrasound peak pressure to ensure the same acoustic energy compared to that of SFFU. Scale bar: 1 mm. *, **, and *** indicate p-values of < 0.05, < 0.01, and < 0.001, respectively.

06 November 2026 22:47:50

© Author(s) 2025

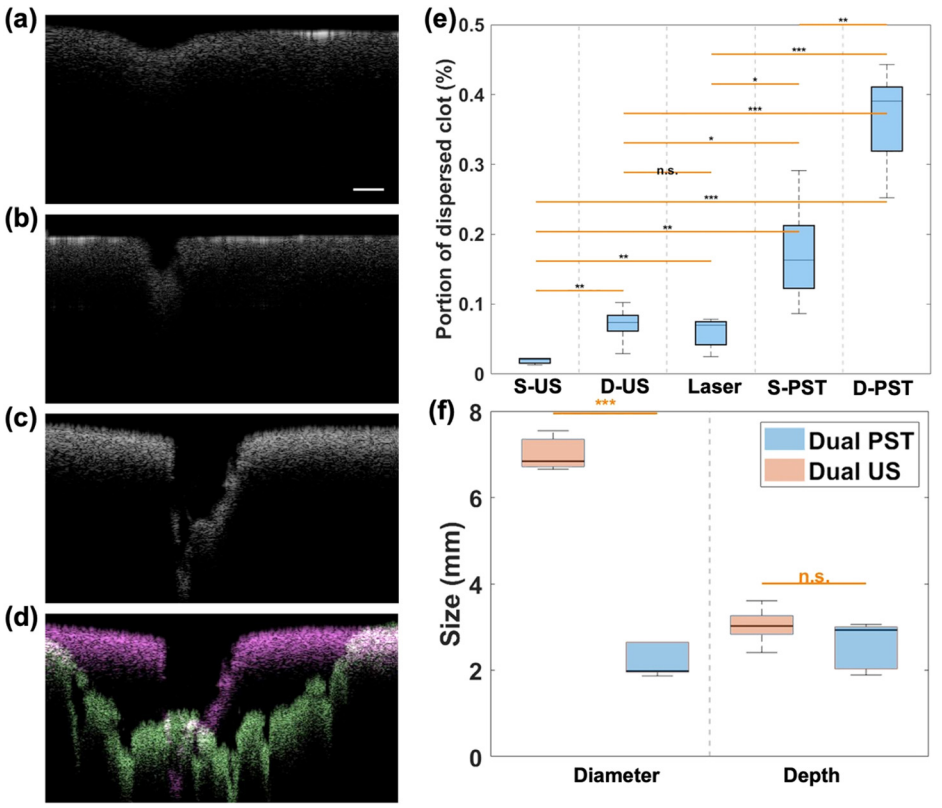


FIG. 4. Thrombolysis enhancement and precision with dual-frequency PST with blood clot phantom. (a)–(c) OCT cross-sectional images of blood clot phantoms after treatment with (a) pulsed laser only ($2\,mJ/cm^2$), (b) dual-frequency ultrasound only (565 kPa), and (c) dual-frequency PST. (d) Comparison of treatment zone profiles between dual-frequency PST (purple) and dual-frequency US only (green). (e) T-test comparison of the portion of dispersed clot across different treatment groups (S-US: single-frequency US only; D-US: dual-frequency US only; Laser: laser only; S-PST: single-frequency PST; D-PST: dual-frequency PST). (**f**) T-test comparison of thrombolysis depth and diameter after dual-frequency PST and ultrasound-only treatment. Scale bar: 1 mm. *,**, and *** indicate p-values of <0.05, <0.01, and <0.001, respectively.

approach holds strong potential to improve the precision and safety of cavitation-based biomedical therapies.

Although previous studies have shown that the frequency difference in dual-frequency ultrasound has a negligible effect in HIFU applications,[16] it should be considered important in PST due to its influence on laser repetition frequency. The mechanism behind dual-frequency ultrasound for enhancing cavitation activities is still poorly understood. One contributing factor may be the increased peak negative pressure, which raises the proportion of the acoustic cycle exceeding the cavitation threshold.[16] Additionally, the broader frequency content may activate a wider range of bubble nuclei sizes.[22] When synchronized with pulsed laser-generated photoacoustic waves, it will significantly improve the triggered bubble nucleation.[23]

In addition, the Keller–Miksis model was employed to simulate the dynamics of single bubbles under various laser and ultrasound conditions. Prior studies have shown that dual-frequency ultrasound can lower the cavitation threshold, and that combining pulsed laser with single-frequency ultrasound bursts significantly increases the maximum bubble radius.[23–25] In this study, we further integrated pulsed laser excitation with dual-frequency ultrasound, providing additional evidence that this combination facilitates enhanced inertial cavitation and improved treatment efficacy. However, several factors remain to be addressed to further refine our simulation model. First, light propagation within biological tissue—particularly scattering and absorption—should be modeled more realistically, especially in the context of vessel geometry. Because the nanosecond laser pulse induces photoacoustic waves that affect the negative peak pressure when combined with the ultrasound burst, this interaction can influence the cavitation threshold and ultimately affect therapeutic outcomes. Second, thermal effects induced by both laser and ultrasound should be considered, not only for safety evaluation but also because temperature changes can alter cavitation thresholds.[26]

Furthermore, our experimental results show that the treatment area in PST can be effectively confined by the laser beam size, addressing a key limitation of low-frequency focused ultrasound, which typically produces a larger and less confined focal zone. In our system, a Gaussian laser beam with a diameter of approximately 2 mm was used, and the effective treatment area was limited to ~1 mm within the laser spot under our experimental parameters. Furthermore, the treatment depth can be precisely controlled by adjusting the delay time between the laser pulse and the ultrasound burst. Together, these results suggest that adaptive control over ultrasound power, laser fluence, and laser–ultrasound synchronization timing could enable personalized and depth-specific therapies tailored to vessel size and location. Finally, OCT and OCTA provide a powerful monitoring tool to evaluate the performance of PST, enabling measurement of *in vivo* vessel diameter and density across different tissue depths.[27] In conventional laser-based treatments, initial vessel conditions—such as diameter and depth—are known to significantly influence treatment outcomes.[28] In contrast, PST appears less sensitive to these variations, as ultrasound energy can penetrate deeper into the tissue and maintain relatively consistent performance across different vessel sizes. This makes PST particularly well-suited for targeting vessels of varying diameters at greater tissue depths. However, the imaging depth of our current

06 November 2026 22:47:50

© Author(s) 2025

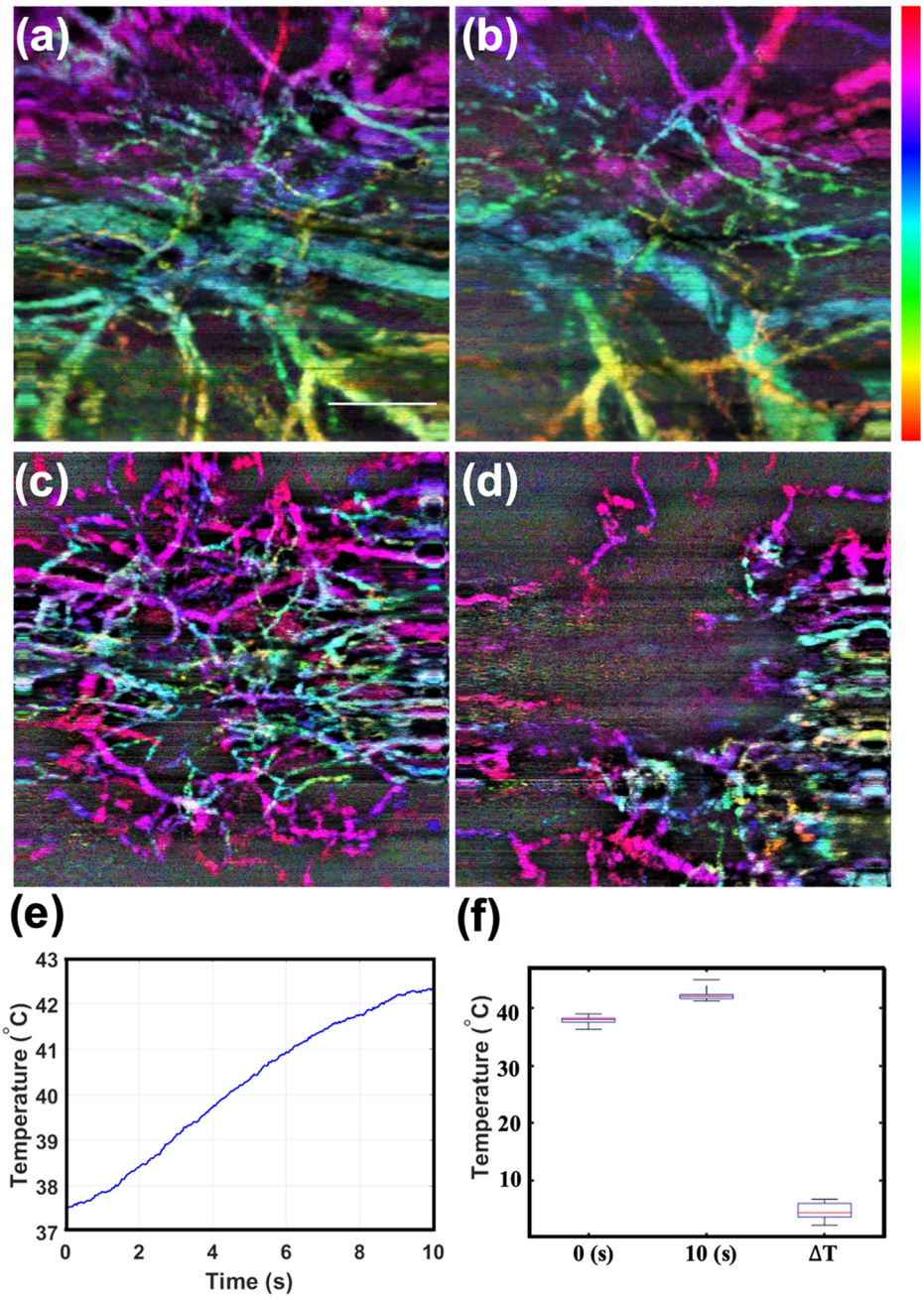


FIG. 5. Projection view of the OCTA image for all layers in the rabbit ear, with depth color-coded for evaluation of vascular disruption. Before (a) and after (b) dual-frequency US-only treatment. Before (c) and after (d) dual-frequency PST treatment. Temperature change during PST in 10 s (e) and (f). 0(s): initial temperature before PST; 10(s): final temperature after PST; ΔT: temperature change. Scale bar: 1 mm. Color bar shows depths from 0 to 900 nm (red to pink).

OCTA system is approximately 900 μm, and the PST treatment depth exceeds the imaging capacity of the current OCTA system. In our rabbit experiments, treatment success was defined by a significant decrease in BVD. In the future, the efficacy of PST should be further evaluated across vessels of different diameters and depths, including distinctions between arteries and veins. Such investigations will be critical to optimizing treatment protocols for personalized and vessel-specific therapy.

METHODS

Setup

The PST system integrates a 500 kHz focused ultrasound transducer with a focal width of 3.02 mm (H-107, Sonic Concepts, WA, USA) and a 532 nm nanosecond pulsed laser (DCH-532-10, NY, USA). Ultrasound bursts are generated using a function generator, producing either a 500 kHz sine wave (for single-frequency excitation) or a combined 500 and 525 kHz sine wave (for dual-frequency

06 November 2026 22:47:50

© Author(s) 2025

TABLE I. Success rates of vascular disruption in rabbit ear under different treatment conditions.

Group	Total spots	Successful spots	Successful rate (%)
Laser only	6	0	0
Single-frequency US	6	0	0
Dual-frequency US	6	0	0
Single-frequency PST	6	3	50
Dual-frequency PST	6	5	83

excitation). The signal is routed through an impedance-matching circuit (H107 Matching Network, Sonic Concepts, WA, USA) and amplified by a 49 dB power amplifier before delivery to the target. A pulse/receiver is used to measure the time delay between the laser and ultrasound signals, and a delay generator ensures precise synchronization.

The SS-OCT system employs a MEMS-tunable vertical cavity surface emitting laser (VCSEL) swept source (SL1310V1, Thorlabs, NJ, USA) with a central wavelength of 1310 nm, a sweep rate of 100 kHz, and a spectral bandwidth of 100 nm. The balanced detector (PDB480C-AC, Thorlabs, NJ, USA) operates in the 1200–1700 nm range with a 1.6 GHz bandwidth. The system achieves a sensitivity of ~110 dB, an axial resolution of ~9 μm, and a lateral resolution of ~30 μm.

A double-clad fiber was used to integrate the PST and OCT system, enabling OCT light propagation through the single-mode core while delivering laser pulses via the multimode inner cladding. The light beam was then focused confocally with the ultrasound focal zone through an objective lens. A specially designed conical holder filled with degassed, double-distilled water served as an acoustic coupling medium, featuring a central hole to allow optical transmission. OCT imaging was performed both before and after PST treatment, conducted without the cone holder in place. To measure temperature changes during PST, a FLIR A300 thermal imaging camera was used at 30 Hz.

Simulation on cavitation threshold

Cavitation activities during PST were simulated using the Keller–Miksis model, which describes the radial dynamics of a single gas bubble in a compressible liquid under varying acoustic and laser-induced pressure conditions. The form of the equation is as follows:

$$\left(1-\frac{\dot{R}}{c}\right)R\ddot{R}+\frac{3}{2}\left(1-\frac{\dot{R}}{3c}\right)\dot{R}^2 = \frac{R}{\rho c}\frac{d}{dt}[P_B]+\frac{1}{\rho}\left(1+\frac{\dot{R}}{c}\right)\left(P_B-P_\infty-p\left(t+\frac{R}{c}\right)\right), \quad (1)$$

where R is the bubble radius, $\dot{R}$ and $\ddot{R}$ are the first and second time derivatives of the radius, c is the sound speed in the surrounding medium, ρ is the density of the surrounding medium, P_∞ is the pressure at infinity, P_B is the pressure at the surrounding medium side of the interface between the medium and the bubble,

$$P_B=\left(P+\frac{2\sigma}{R_0}\right)\left(\frac{R_0}{R}\right)^{3k}-\frac{2\sigma}{R}-\frac{4\mu}{R}\dot{R}, \quad (2)$$

where σ is the surface tension coefficient, μ is the viscosity of the fluid, and k is the polytropic index. Here, we assume the values of $k, \rho, P_\infty, \sigma, \mu$, and c to be 1.4, 1055 $\frac{\text{kg}}{\text{m}^3}$, 104.6 kPa, 0.072 $\frac{\text{N}}{\text{m}}$, 0.005 Pa s, and 1500 m/s.[21] The initial bubble radius (R_0) was assumed to be 50–200 nm. $p\left(t+\frac{R}{c}\right)$ in Eq. (1) is the applying pressure, which is composed of the applied ultrasound pressure p_{US} and the photoacoustic (PA) pressure p_{PA} induced by the pulse laser,

$$p = p_{US}+p_{PA}. \quad (3)$$

The p_{PA} is the pressure of the thermo-elastic pressure wave generated due to nanosecond laser pulse absorbed by the medium. The initial pressure at the laser focused position inside the vessel is given by

$$p_{0_{PA}}(r)=\Gamma\mu_a F(r), \quad (4)$$

where Γ is the Gruneisen constant, μ_a is the optical absorption coefficient, and $F(r)$ is the laser fluence. For blood, μ_a is 250 cm^{-1} at 532 nm laser wavelength, and Γ is 0.2. Assume the laser pulse with the Gaussian temporal profile, and the pressure wave inside the vessel can be calculated with following equation:

$$p_{PA}(r,t)=\frac{\int_{-\infty}^{+\infty} e^{\left(-\frac{2t'}{T}\right)^2} p_\delta(r,t-t')\mathrm{d}t'}{\int_{-\infty}^{+\infty} e^{\left(-\frac{2t'}{T}\right)^2} dt'}, \quad (5)$$

where p_δ is the pressure wave for delta heating, and T is the laser pulse width defined at the full width of half maximum.

PCD detection

The detection transducer with a center frequency of 10 MHz was used to monitor cavitation activity. The detected ultrasound signals were broadband shock waves generated by bubble collapse, and the signal intensity was used as an indicator of cavitation activity. To eliminate interference from harmonic and subharmonic signals produced by the excitation HIFU transducer, a comb notch filter was applied during the signal processing.

Sample preparation and animal study

In vitro blood clots were prepared using porcine blood anticoagulated with sodium citrate (Sierra for Medical Science, Inc., Whittier, CA, USA). The preparation of coagulation was performed using a modified version of the protocol. To initiate coagulation, calcium chloride ($CaCl_2$) solution at 2.75% w/v was added to the blood at a volume ratio of 5 ml $CaCl_2$ per 50 ml blood. After thorough mixing, the solution was gently transferred into borosilicate glass tubes with 12 mm outer diameter and immediately sealed to prevent contamination. The sealed tubes were incubated in a dry bath at 37 °C for 3 h to promote coagulation. A dry bath incubator was used instead of a water bath to eliminate potential cross-contamination. After incubation, the tubes were transferred to a 4 °C refrigerator and stored for over 72 h to ensure complete clot formation. The resulting clots were cylindrical with a diameter of approximately 10 mm. Prior to thrombolysis experiments, clots were equilibrated in 37 °C saline solution for at least 1 h.

06 November 2026 22:47:50

© Author(s) 2025

In vivo experiments were conducted on the ears of male New Zealand white rabbits. Each animal was initially anesthetized with subcutaneous injection of ketamine (35 mg/kg) and xylazine (5 mg/kg), with the dose adjusted according to body weight. Once a sufficient depth of anesthesia was confirmed via pedal reflex and respiratory rate, the hair on the rabbit's ear was shaved, and target regions were identified for treatment.

ACKNOWLEDGMENTS

The work was supported by the National Institutes of Health (Grant Nos. R01EB-030558, R01HL-125084, R01EY-028662, R01EB-030024, R01HL177188, and UG3DA065120) and the Air Force Office Scientific Research (Grant No. FA9550-23-1-0685).

AUTHOR DECLARATIONS

Conflict of Interest

The authors have no conflicts to disclose.

Ethics Approval

Ethics approval for experiments reported in the submitted manuscript on animal or human subjects was granted. All animal experiments were conducted in accordance with the guidelines approved by the Institutional Animal Care and Use Committee (IACUC) and the Institutional Biosafety Committee (IBC) of University of California, Irvine (protocol #AUP-25–036).

Author Contributions

Yuchen Song and Shuang Wei contributed equally to this work.

Yuchen Song: Conceptualization (lead); Data curation (lead); Formal analysis (lead); Investigation (lead); Methodology (lead); Project administration (equal); Software (lead); Validation (lead); Visualization (lead); Writing – original draft (lead); Writing – review & editing (equal). **Shuang Wei:** Data curation (lead); Validation (lead); Visualization (lead); Writing – original draft (equal); Writing – review & editing (equal). **Haibin Zou:** Data curation (equal); Software (equal); Writing – review & editing (equal). **Jingyi Wang:** Data curation (equal); Visualization (equal); Writing – review & editing (equal). **Fengyi Zhang:** Data curation (equal); Methodology (equal); Writing – review & editing (equal). **Qifa Zhou:** Conceptualization (equal); Supervision (equal); Writing – review & editing (equal). **Yun Jing:** Conceptualization (lead); Methodology (lead); Project administration (lead); Supervision (lead); Writing – review & editing (lead). **Zhongping Chen:** Conceptualization (lead); Funding acquisition (lead); Methodology (lead); Project administration (lead); Supervision (lead); Writing – review & editing (equal).

DATA AVAILABILITY

The data that support the findings of this study are available from the corresponding authors upon reasonable request.

REFERENCES

[1]A. D. Maxwell *et al.*, "Noninvasive thrombolysis using pulsed ultrasound cavitation therapy—Histotripsy," Ultrasound Med. Biol. **35**(12), 1982–1994 (2009).
[2]G. Ter Haar, "HIFU tissue ablation: Concept and devices," Adv. Exp. Med. Biol. **880**, 3–20 (2016).
[3]K. B. Bader *et al.*, "Overview of therapeutic ultrasound applications and safety considerations: 2024 update," J. Ultrasound Med. **44**(3), 381–433 (2025).
[4]M. Wan, Y. Feng, and G. Ter Haar, *Cavitation in Biomedicine* (Springer, The Netherlands, 2015).
[5]Y. Matsumoto *et al.*, "Medical ultrasound with microbubbles," Exp. Therm. Fluid Sci. **29**(3), 255–265 (2005).
[6]C. Coussios *et al.*, "Role of acoustic cavitation in the delivery and monitoring of cancer treatment by high-intensity focused ultrasound (HIFU)," Int. J. Hyperthermia **23**(2), 105–120 (2007).
[7]V. S. Bachu *et al.*, "High-intensity focused ultrasound: A review of mechanisms and clinical applications," Ann. Biomed. Eng. **49**(9), 1975–1991 (2021).
[8]H. Cui, T. Zhang, and X. Yang, "Laser-enhanced cavitation during high intensity focused ultrasound: An *in vivo* study," Appl. Phys. Lett. **102**(13), 133702 (2013).
[9]Y. Li *et al.*, "High speed photo-mediated ultrasound therapy integrated with OCTA," Sci. Rep. **12**(1), 19916 (2022).
[10]Y. Song *et al.*, "Real-time mapping of photo-sono therapy induced cavitation using Doppler optical coherence tomography," Opt. Lett. **49**(17), 4843–4846 (2024).
[11]Y. Qin *et al.*, "The effect of laser and ultrasound synchronization in photo-mediated ultrasound therapy," IEEE Trans. Biomed. Eng. **67**(12), 3363–3370 (2020).
[12]M. Wang *et al.*, "Cutaneous hypervascularization treatment using photo-mediated ultrasound therapy," JID Innovation **3**(6), 100237 (2023).
[13]R. Feng *et al.*, "Enhancement of ultrasonic cavitation yield by multi-frequency sonication," Ultrason. Sonochem. **9**(5), 231–236 (2002).
[14]S. Guo, Y. Jing, and X. Jiang, "Temperature rise in tissue ablation using multi-frequency ultrasound," IEEE Trans. Ultrason. Ferroelectr. Freq. Control **60**(8), 1699–1707 (2013).
[15]D. Zhang *et al.*, "Multi-frequency therapeutic ultrasound: A review," Ultrason. Sonochem. **100**, 106608 (2023).
[16]D. Suo *et al.*, "Thrombolysis using multi-frequency high intensity focused ultrasound at MHz range: An *in vitro* study," Phys. Med. Biol. **60**(18), 7403 (2015).
[17]D. Suo *et al.*, "Microbubble mediated dual-frequency high intensity focused ultrasound thrombolysis: An *in vitro* study," Appl. Phys. Lett. **110**(2), 023703 (2017).
[18]S. Moon *et al.*, "A dual-frequency intravascular ultrasound transducer for amplified nanodroplet vaporization effects in cavitation-enhanced sonothrombolysis," in *IEEE International Ultrasonics Symposium (IUS)* (IEEE, 2022), pp. 1–4.
[19]H. Wu *et al.*, "Dual-frequency intravascular sonothrombolysis: An *in vitro* study," IEEE Trans. Ultrason. Ferroelectr. Freq. Control **68**(12), 3599–3607 (2021).
[20]X. Yang and C. C. Church, "A model for the dynamics of gas bubbles in soft tissue," J. Acoust. Soc. Am. **118**(6), 3595–3606 (2005).
[21]R. Singh, X. Wang, and X. Yang, "Cavitation induced shear and circumferential stresses on blood vessel walls during photo-mediated ultrasound therapy," AIP Adv. **10**(12), 125227 (2020).
[22]P. Ciuti *et al.*, "Study into mechanisms of the enhancement of multibubble sonoluminescence emission in interacting fields of different frequencies," Ultrason. Sonochem. **10**(6), 337–341 (2003).
[23]R. Singh and X. Yang, "Cavitation induced shear and circumferential stresses on blood vessel walls during photo-mediated ultrasound therapy," AIP Adv. **12**(4), 045020 (2022).
[24]D. Suo *et al.*, "Numerical investigation of the inertial cavitation threshold under multi-frequency ultrasound," Ultrason. Sonochem. **41**, 419–426 (2018).
[25]Z. Li, Q. Zou, and D. Qin, "Enhancing cavitation dynamics and its mechanical effects with dual-frequency ultrasound," Phys. Med. Biol. **67**(8), 085017 (2022).
[26]E. Vlaisavljevich *et al.*, "Effects of temperature on the histotripsy intrinsic threshold for cavitation," IEEE Trans. Ultrason. Ferroelectr. Freq. Control **63**(8), 1064–1077 (2016).
[27]J. Wang *et al.*, "Miniaturized head-mount doppler optical coherence tomography scope for freely moving mouse," ACS Photonics **11**(8), 3381–3389 (2024).
[28]L. O. Svaasand *et al.*, "Therapeutic response during pulsed laser treatment of port-wine stains: Dependence on vessel diameter and depth in dermis," Lasers Med. Sci. **10**(4), 235–243 (1995).

06 November 2026 22:47:50

© Author(s) 2025